Spatial calibration and image processing requirements of an image fiber bundle based snapshot hyperspectral imaging probe: From raw data to datacube

Hoong-Ta Lim*, Murukeshan Vadakke Matham
Centre for Optical and Laser Engineering (COLE), School of Mechanical and Aerospace Engineering, Nanyang Technological University (NTU), Singapore 639798
*Email: limht@ntu.edu.sg

ABSTRACT

Hyperspectral imaging was first used in remote sensing and since then, it has been used in many other applications such as cancer diagnosis, precision farming and assessment of the level of flaking in ancient murals. In order to make hyperspectral imaging available for a wide variety of applications, its imagers can be made to operate using different methods and developed into different configurations. This leads to each variant having a set of specifications suitable for certain applications. The many variants of hyperspectral imager produce a set of three-dimensional spatial-spatial-spectral datacube, which is made up of hundreds of spectral images of one scene. A snapshot hyperspectral imaging probe has recently been developed by integrating a fiber bundle, which is made up of specially-arranged optical fibers, with a spectrograph-based hyperspectral imager. The snapshot method is able to produce a datacube using the information from each scan. The fiber bundle has 100 fiberlets which are arranged in a row in the one-dimensional proximal end, and are rearranged into a 10×10 hexagonal array in the two-dimensional distal end. The image captured by the two-dimensional end of the fiber bundle is reduced from two to one spatial dimension at the one-dimensional end. The raw data acquired from each scan has to be remapped into a datacube with the correct representation of the spectral and spatial features of the captured scene. This paper reports the spatial calibrations of both ends of the fiber bundle and image processing that have to be performed for such a remapping.

Keywords: Hyperspectral imaging, fiber bundle, snapshot, image processing, datacube.

1. INTRODUCTION

There are many new optical configurations and related instrumentations reported in the recent past exploiting bulk optics and fiber optics concepts targeting applications in lithography,[1-4] communications[5, 6] and imaging.[7-11] Hyperspectral imaging (HSI) combines imaging and spectroscopy to give many images of the same scene at contiguous and narrow wavelength bands.[12] Therefore, detailed spectral fingerprint can be acquired from each spatial position in the imaged scene. The information acquired can be represented as a three-dimensional (3D) spatial-spatial-spectral dataset, which is also known as a datacube.[13] By using algorithms such as spectral unmixing and principal component analysis to perform classification and quantification, the datacube can be analyzed to reveal important information of the scene.[14] HSI has been used to differentiate between healthy tissue and cancerous tumors,[15, 16] precision farming[17] and assessment of the level of flaking in ancient murals.[18]

Optical fibers have been used for health monitoring of structures[19] and endoscopic bio-imaging applications[11] for diseases occurring at sites within the body that are not easily accessible by conventional table-top setup. Hyperspectral (HS) endoscopes have been developed to satisfy the medical needs to perform HSI of the human body from within. HS endoscopes have appeared in different configurations, using spatial-scanning, spectral-scanning and snapshot methods.[20-22] These imagers have different characteristics and can be selected based on the imaging specifications and applications. Unlike spatial-scanning and spectral-scanning HS imagers, a snapshot HS imager is able to form a datacube from each scan. Motion artifacts and pixel misregistration in a snapshot imager can therefore be eliminated.[7] Snapshot HS imager does not need to perform repeated scanning to form a datacube, and thus is preferred in real-time endoscopic applications such as *in vivo* disease diagnosis and surgical monitoring. Until recently, snapshot HS imager has only been developed using the concept of image mapping spectroscopy.[22] It has an image mapper which plays a key role by spatially distributing light from neighboring regions of the sample to isolated regions on the sensor array of the detector camera.

Fifth International Conference on Optical and Photonics Engineering, edited by Anand Krishna Asundi,
Proc. of SPIE Vol. 10449, 104491P · © 2017 SPIE · CCC code: 0277-786X/17/$18
doi: 10.1117/12.2270739

An endoscopic snapshot HS imager using the concept of integral field spectroscopy (IFS) has recently been adopted.[23] IFS uses a reformatter that comes in different forms such as fiber bundle, box and rod.[24, 25] The fiberlets on one end of the reformatter are arranged in a two-dimensional (2D) array, and the fiberlets on the other end are arranged in a one-dimensional (1D) row.[26] Light from the 2D scene is captured by the fiberlets on the 2D end of the reformatter, and through the fiberlets, the light is transferred to the 1D end.[27] The use of such a reformatter in a HS imager allows the 2D sensor array to capture 3D spatial-spatial-spectral data of the scene, to become a snapshot configuration. However, the 2D spatial information of the fiberlets on the 2D end is lost and therefore there is a need to perform spatial calibrations of the fiberlets on both ends of the fiber bundle. Image processing is also required. These allow the spectra from the fibers on the 1D end to be correctly remapped to the corresponding positions on the 2D end, for the visualization of the data.

The endoscopic snapshot HS imager which is recently reported adopts the concept of IFS and uses a reformatter in a form of a fiber bundle.[23] The custom-fabricated 2D to 1D fiber bundle is flexible along its length and its distal end has a small profile so that it serves another function of being an endoscope to be inserted into the orifice of body cavities.[28] It has 100 fiberlets that are arranged in a 10×10 hexagonal array on the 2D end, which are then arranged in a row of fiberlets on the 1D end. Fiberlet 4 is inactive and thus it cannot be used for imaging. This paper focuses on the strategy adopted for the spatial calibrations of both ends of the fiber bundle and image processing that have to be performed so that the raw data in each scan can be correctly remapped to form a datacube.

2. EXPERIMENTAL SETUP

The experimental setup is the same as earlier reported.[23] The system captures 756 wavelength bands within the spectral range from 400 nm to 1000 nm.[29] Imaging was done in reflectance mode using a broadband light source (MI-150, Edmund Optics). The sample is a phantom tissue with a black tape on it (Figure 1). It was moved towards the right using a mechanical stage during imaging. All imaged objects were placed at ~0.5 mm away from the 2D end-face of the fiber bundle. Images were acquired at a rate of ~6.16 Hz. All data and image processing was done offline using MATLAB®.

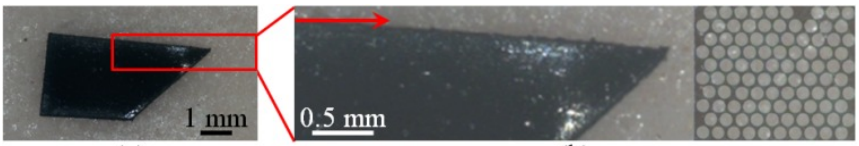

Figure 1: (a) Phantom tissue sample and (b) imaged region with photograph of 2D end of fiber bundle superimposed.

3. SPATIAL CALIBRATIONS

3.1 Spatial calibration on 1D end of fiber bundle

The spatial calibration on the 1D end of the fiber bundle was conducted while the 2D end was imaging a 99% reflectance standard (SRS-99-010, Labsphere). The 2D spatial-spectral image of the 1D end of the fiber bundle is captured by the detector camera (Figure 2) and investigated. The 1004 pixel columns of the sensor array are used to image the 100 fiberlets. Each colored vertical line in Figure 2 came from the light exiting the core of each fiberlet, and spectrally dispersed in the vertical direction (along *y*-axis).

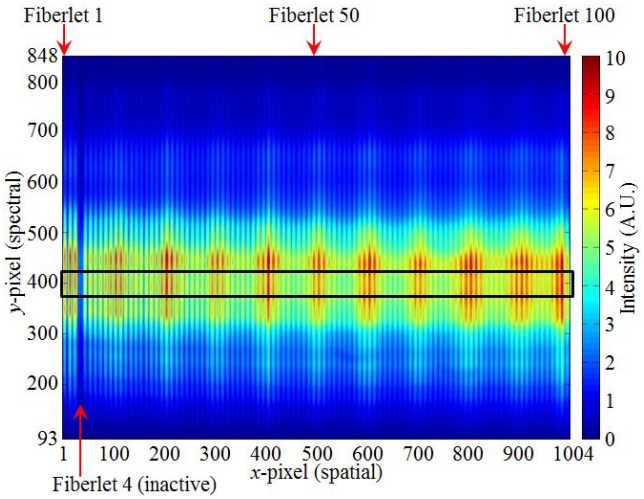

Figure 2: 2D spatial-spectral image of 1D end of fiber bundle taken by detector camera.

The *x*-pixel used to image the center of each fiberlet is determined using Figure 2. From the 2D spatial-spectral image, an intensity plot [Intensity (A.U.) vs *x*-pixel)] is acquired from the region indicated by the black rectangle in Figure 2 after performing vertical averaging of the data in this region. The resulting intensity plot is a signal of peaks and valleys, with the *x*-pixel of each peak correspond to the center of each fiberlet. The *x*-pixel of each peak in the intensity plot is determined using the "findpeaks" function in MATLAB®.

3.2 Spatial calibration on 2D end of fiber bundle

The spatial calibration on the 2D end of the fiber bundle was conducted by first taking a photograph of the 2D end-face when the 100 fiberlets on the1D end are illuminated [Figure 3(a)]. The bright circular regions in Figure 3(a) are the cores of the fiberlets, which are used for imaging. Next, a binary mask of the 2D end-face was created where bright pixels are denoted as "1" while dark pixels are denoted as "0". Using the binary mask, the authors defined a rectangular region surrounding the core of each fiberlet. Within each rectangular region where the pixels are denoted as "1", these pixels are relabeled according to the order of the fiberlets on the 1D end. This forms the digital mask of the 2D end-face of the fiber bundle [Figure 3(b)]. Since Fiberlet 4 is inactive and cannot be used for imaging, the position of its core is not included in the digital mask.

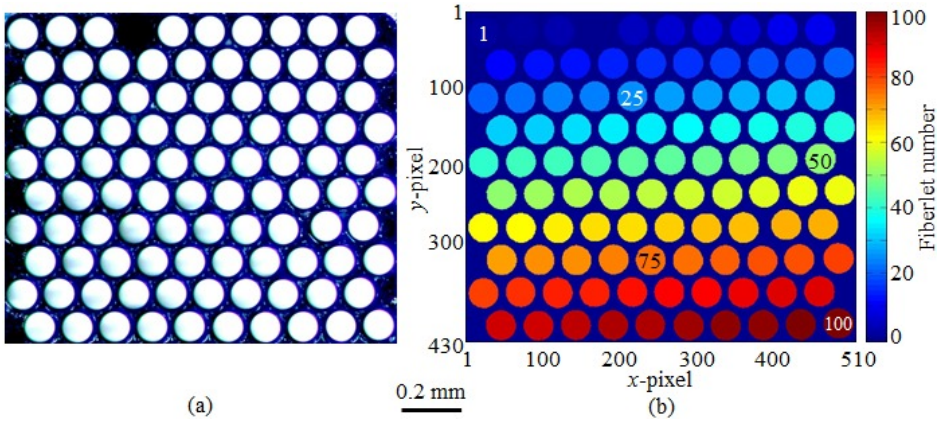

Figure 3: (a) Photograph and (b) digital mask of 2D end-face of fiber bundle.

When light from the scene enters the fiber bundle from the 2D end and then exits from the 1D end, the 2D spatial information of the scene is lost. These spatial calibrations are conducted so that the spectrum acquired from each fiberlet on the 1D end can be remapped according to its position on the 2D end.

4. IMAGE PROCESSING

4.1 2D spatial-spectral reflectance image

Sample data were acquired from the phantom tissue sample and were corrected using white reference (*White*) and dark reference (*Dark*) using Eq. (1) to get the *Reflectance* data. A total of 80 images (*Frame*) of the sample were acquired. *White* data were acquired by imaging the 99% reflectance standard (SRS-99-010, Labsphere), where the reflectance was 99%. *Dark* data were acquired when the forelens was covered. It represents the image with dark current noise where the reflectance was 0%. A set of ten images were taken and averaged to give the *White* and *Dark* data. x and λ refer to the column and the calibrated spectral band allocated to the row of the sensor array, respectively. This results in a 1004×756 spatial-spectral reflectance image for each frame (Figure 4).

$$Reflectance(x,\lambda,Frame) = \frac{Sample(x,\lambda,Frame) - Dark(x,\lambda)}{White(x,\lambda) - Dark(x,\lambda)} \times 0.99. \quad (1)$$

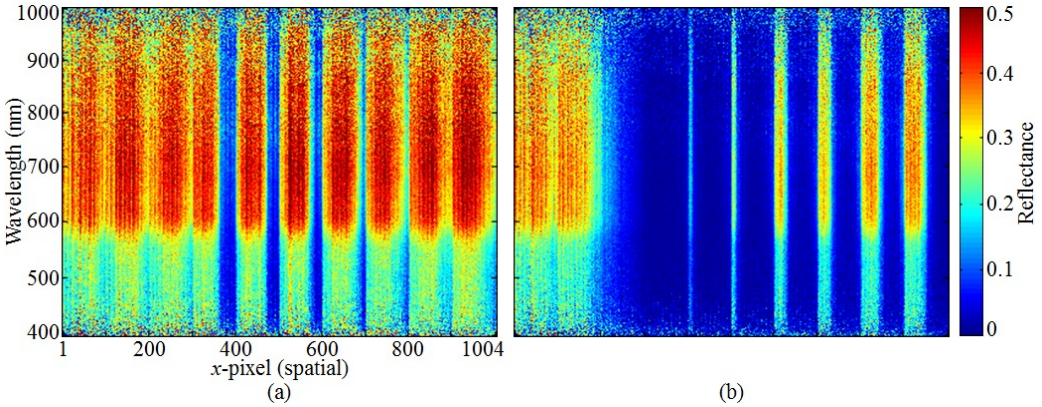

Figure 4: 2D spatial-spectral reflectance images of (a) Frame 21 and (b) Frame 44.

4.2 2D fiberlet-spectral reflectance image

1004 *x*-pixels were used to image the 100 fiberlets on the 1D end of the fiber bundle. Therefore ~10 *x*-pixels were used to image each fiberlet. Using the known *x*-pixel position used to image the core center of each fiberlet (Sec. 3.1), the reflectance data from seven *x*-pixel positions were used for each fiberlet. These seven *x*-pixel positions are from the *x*-pixel position used to image the core center as well as the six nearest beside it (three on the left and right). The spectra from each group of seven *x*-pixel positions are then averaged to give a reflectance spectrum. This is followed by a 9-point moving average of the spectrum for smoothing. The spectrum for Fiberlet 4 is set to zero since it is inactive and cannot be used for imaging. This results in a 100×756 fiberlet-spectral reflectance image for each frame (Figure 5).

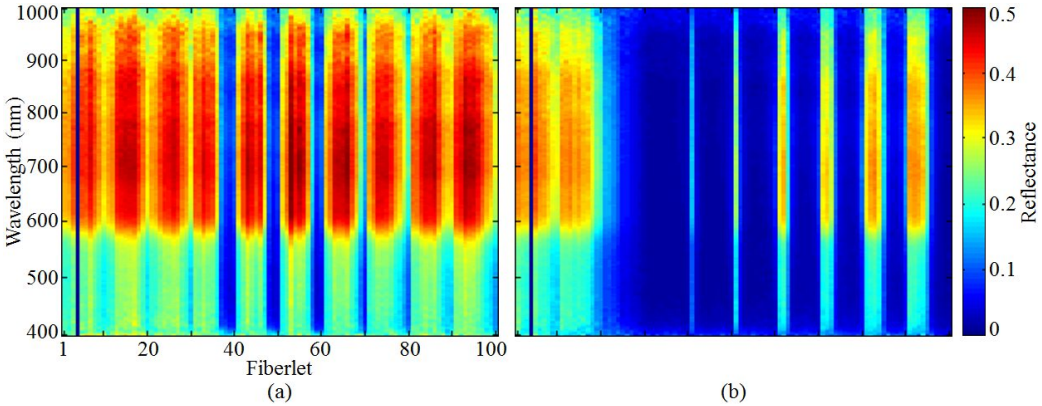

Figure 5: 2D fiberlet-spectral reflectance images of (a) Frame 21 and (b) Frame 44.

4.3 Remapping of 2D fiberlet-spectral reflectance image into 3D datacube

The photograph used to create the digital mask, as shown in Figure 3, was taken when the 2D end-face of the fiber bundle was facing the camera. During imaging of the sample, the 2D end is orientated such that the left side of the fiber

bundle (as shown in Figure 3) is used to image the right side of the sample. Therefore prior to creating the 3D datacube, the digital mask has to be flipped horizontally. The spectral data in Sec. 4.2 are then remapped according to the location of the core of the respective fiberlet in the flipped digital mask to form a 3D 510×430×756 spatial-spatial-spectral datacube for each frame. Cut-datacubes are shown in Figure 6 so that the internal features of the datacubes are revealed. Reflectance mappings can then be acquired by taking horizontal slices of the datacubes (Figure 7). The features shown in the reflectance mappings are the correct representation of the features in the captured scene, as shown in Figure 1. It is also observed that the sample was moving towards the right from Frame 21 to Frame 44. This correctly reveals the actual sample movement during imaging.

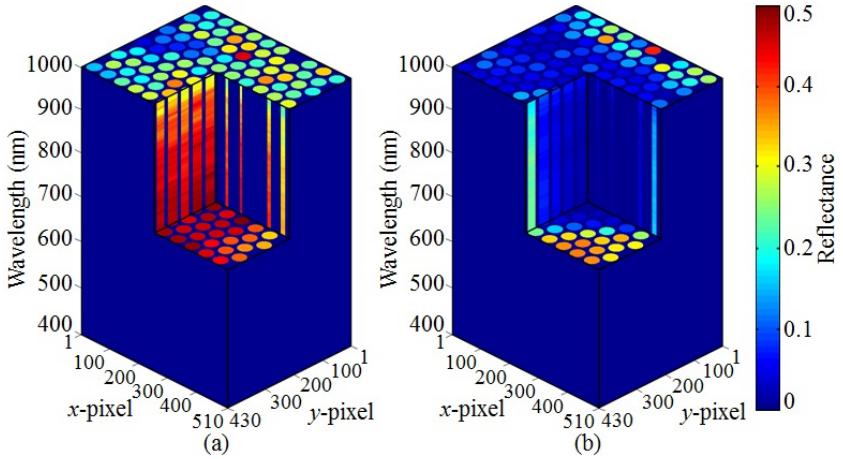

Figure 6: 3D spatial-spatial-spectral datacubes of (a) Frame 21 and (b) Frame 44.

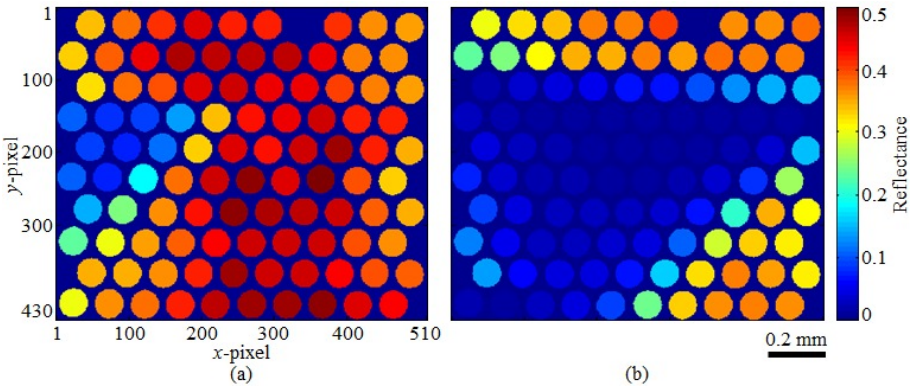

Figure 7: 700-nm reflectance mappings of (a) Frame 21 and (b) Frame 44.

5. CONCLUSION

An endoscopic snapshot HS imager using the concept of IFS has recently been reported.[23] A custom-fabricated 2D to 1D fiber bundle with 100 fiberlets is used as a reformatter to perform spatial transformation of the scene. The number of spatial dimension of the scene is reduced from two to one when the light exits the 1D end of the fiber bundle. This makes it a snapshot configuration as the full data of the scene is acquired by the detector camera in one scan. By making the fiber bundle flexible along its length with a distal end of a small profile, it serves another function of being an endoscope. The paper gave a detailed account on the spatial calibrations and image processing that are conducted for such a reformatter, so that the raw data in each scan is remapped into a 3D datacube. The results show that these procedures have been successfully implemented to show the features and movement of the sample.

The authors acknowledge the financial support received through MOE (RG 98/14 and RG 162/15) and COLE-EDB funding.

REFERENCES

[1] M. Tang *et al.*, "Maskless multiple-beam laser lithography for large-area nanostructure/microstructure fabrication," Appl. Opt. 50(35), 6536-6542 (2011).

[2] V. M. Murukeshan, and K. V. Sreekanth, "Excitation of gap modes in a metal particle-surface system for sub-30 nm plasmonic lithography," Opt. Lett. 34(6), 845-847 (2009).

[3] K. V. Sreekanth, and V. M. Murukeshan, "Large-area maskless surface plasmon interference for one- and two-dimensional periodic nanoscale feature patterning," J. Opt. Soc. Am. A-Opt. Image Sci. Vis. 27(1), 95-99 (2010).

[4] K. Sreekanth, V. Murukeshan, and J. Chua, "A planar layer configuration for surface plasmon interference nanoscale lithography," Appl. Phys. Lett. 93(9), 093103 (2008).

[5] T. Fehenberger *et al.*, "On achievable rates for long-haul fiber-optic communications," Opt. Express 23(7), 9183-9191 (2015).

[6] P. Prabhathan *et al.*, "Discrete and fine wavelength tunable thermo-optic WSS for low power consumption C+L band tunability," IEEE Photonics Technol. Lett. 24(2), 152-154 (2012).

[7] W. R. Johnson *et al.*, "Snapshot hyperspectral imaging in ophthalmology," J. Biomed. Opt. 12(1), 014036 (2007).

[8] U. Dinish *et al.*, "Formulation and implementation of a phase-resolved fluorescence technique for latent-fingerprint imaging: theoretical and experimental analysis," Appl. Opt. 44(3), 297-304 (2005).

[9] A. Kishen *et al.*, "Analysis on the nature of thermally induced deformation in human dentine by electronic speckle pattern interferometry (ESPI)," J. Dent. 29(8), 531-537 (2001).

[10] N. K. K. Mohan *et al.*, "Separation of the influence of in-plane displacement in multiaperture speckle shear interferometry," Opt. Eng. 33(6), 1973-1982 (1994).

[11] V. K. Shinoj *et al.*, "Design, fabrication, and characterization of thermoplastic microlenses for fiber-optic probe imaging," Appl. Opt. 53(6), 1083-1088 (2014).

[12] Q. Li *et al.*, "AOTF based molecular hyperspectral imaging system and its applications on nerve morphometry," Appl. Opt. 52(17), 3891-3901 (2013).

[13] N. Hagen *et al.*, "Snapshot advantage: a review of the light collection improvement for parallel high-dimensional measurement systems," Opt. Eng. 51(11), 111702 (2012).

[14] G. Lu, and B. Fei, "Medical hyperspectral imaging: A review," J. Biomed. Opt. 19(1), 010901 (2014).

[15] S. Kiyotoki *et al.*, "New method for detection of gastric cancer by hyperspectral imaging: A pilot study," J. Biomed. Opt. 18(2), 026010 (2013).

[16] S. G. Kong, M. Martin, and T. Vo-Dinh, "Hyperspectral fluorescence imaging for mouse skin tumor detection," ETRI J. 28(6), 770-776 (2006).

[17] N. Gat, "Imaging spectroscopy using tunable filters: A review," Proc. SPIE 4056, 50-64 (2000).

[18] M. Sun *et al.*, "What's wrong with the murals at the Mogao Grottoes: A near-infrared hyperspectral imaging method," Sci. Rep. 5, 14371 (2015).

[19] V. M. Murukeshan *et al.*, "On-line health monitoring of smart composite structures using fiber polarimetric sensor," Smart Mater. Struct. 8(5), 544-548 (1999).

[20] H.-T. Lim, and V. M. Murukeshan, "Spatial-scanning hyperspectral imaging probe for bio-imaging applications," Rev. Sci. Instrum. 87(3), 033707 (2016).

[21] M. E. Martin *et al.*, "Development of an advanced hyperspectral imaging (HSI) system with applications for cancer detection," Ann. Biomed. Eng. 34(6), 1061-1068 (2006).

[22] R. T. Kester *et al.*, "Real-time snapshot hyperspectral imaging endoscope," J. Biomed. Opt. 16(5), 056005 (2011).

[23] H.-T. Lim, and V. M. Murukeshan, "A four-dimensional snapshot hyperspectral video-endoscope for bio-imaging applications," Sci. Rep. 6, 24044 (2016).

[24] D. W. Fletcher-Holmes, and A. R. Harvey, "Snapshot foveal hyperspectral imager," Proc. SPIE 4816, 407-414 (2002).

[25] N. Gat *et al.*, "Development of four-dimensional imaging spectrometers (4D-IS)," Proc. SPIE 6302, 63020M (2006).

[26] D. Ren, and J. Allington-Smith, "On the application of integral field unit design theory for imaging spectroscopy," Publ. Astron. Soc. Pac. 114(798), 866-878 (2002).

[27] M. P. Nelson, and M. Myrick, "Fabrication and evaluation of a dimension-reduction fiberoptic system for chemical imaging applications," Rev. Sci. Instrum. 70(6), 2836-2844 (1999).

[28] H.-T. Lim, and V. M. Murukeshan, "Note: Design considerations and characterization of a flexible snapshot hyperspectral probe," Rev. Sci. Instrum. 88(3), 036107 (2017).

[29] H.-T. Lim, and V. M. Murukeshan, "Pushbroom hyperspectral imaging system with selectable region of interest for medical imaging," J. Biomed. Opt. 20(4), 046010 (2015).